Heliyon 10 (2024) e26244

Contents lists available at ScienceDirect

Heliyon

journal homepage: www.cell.com/heliyon

Research article

Polymerized stimuli-responsive microgel hybrids of silver nanoparticles as efficient reusable catalyst for reduction reaction

Biswajit Pany [a,b], Amrito Ghosh Majumdar [b], Suresh Bhat [c], Satybrata Si [a,b], Junpei Yamanaka [d], Priti S. Mohanty [a,b,*]

[a] School of Chemical Technology, Kalinga Institute of Industrial Technology (KIIT), Deemed to be University, Bhubaneswar, 751024, India
[b] School of Biotechnology, Kalinga Institute of Industrial Technology (KIIT), Deemed to be University, Bhubaneswar, 751024, India
[c] Polymer Science & Engineering Division, CSIR-National Chemical Laboratory, Pune, 411008, India
[d] Graduate School of Pharmaceutical Sciences, Nagoya City University, 3-1 Tanabe-dori, Mizuho-ku, Nagoya, 467-8603, Japan

ARTICLE INFO

Keywords:
Stimuli-responsive microgels
Microgel-metal hybrids
PNIPAM microgels
Polymerized hydrogel matrix(PGM
Nanomaterial catalysts
Light scattering

ABSTRACT

We have showcased the potential of polymerized hydrogels (PGMs) with uniform-sized stimuli-responsive microgel particles as promising alternatives to prevent aggregation in solution based nanoparticle systems. In the current work, we implemented the PGM concept by embedding anionic stimuli-responsive microgels (PNIPAM-co-AAc)-silver (Ag) hybrids within a hydrogel matrix. These PGM@AgNP hybrid materials are used as catalysts for the reduction of 4-nitrophenol (4-NP) to 4-aminophenol (4-AP) in the presence of sodium borohydride. UV-VIS spectroscopy is used for studying catalytic activity. In the solution based system, the complete reduction of 4-NP to 4-AP took 30 minutes with pure Ag nanoparticles, 24 minutes with PNIPAM-Ag hybrid (Neutral) microgels and 15 minutes with PNIPAM-co-AAc-Ag (Anionic) hybrid microgels. In contrast PGM containing PNIPAM-co-AAc-Ag hybrids achieved full reduction in just 15 minutes, along with a 3-minute induction period. For pure Ag nanoparticles, the first-order rate constant is found to be 0.25 min^{-1}, for PNIPAM-Ag hybrid (Neutral), it is 0.21 min^{-1} and for PNIPAM-co-AAc-Ag (Anionic), it is 0.5 min^{-1} where as for PGM containing anionic microgel hybrids it is found to be 0.8 min^{-1}. Furthermore, the reusability of the PGM-Ag (anionic) materials for catalytic activity remains unaltered even after several washings. In summary, our study highlights the effectiveness of PGM@AgNP materials as efficient catalysts for the reduction of 4-nitrophenol to 4-aminophenol, indicating their versatile potential in various catalytic applications.

1. Introduction

In recent years, stimuli-responsive poly(N-isopropyl acrylamide) (PNIPAM) microgels have emerged as a popular model system for studying various fundamental problems [1–8]. These microgels have also found widespread use in different applications such as drug delivery, tissue engineering, diagnostics, and separation and purification processes [9–15]. PNIPAM-based microgels are cross-linked polymers that undergo a reversible volume phase transition (VPT) in response to different stimuli parameters such as temperature, pH, and ionic strength [1–8]. This property makes them highly versatile and adaptable to various environmental conditions.

* Corresponding author, School of Chemical Technology and Biotechnology, Kalinga Institute of Industrial Technology (KIIT), Deemed to be University, Bhubaneswar, 751024, India.
E-mail address: pritisundar.mohanty@kiitbiotech.ac.in (P.S. Mohanty).

https://doi.org/10.1016/j.heliyon.2024.e26244
Received 31 December 2023; Received in revised form 5 February 2024; Accepted 8 February 2024
Available online 22 February 2024

In addition to their responsive behavior, there is considerable interest in using cross-linked PNIPAM microgels as microreactors for incorporating different types of metals (e.g., silver, gold, iron) and semiconducting nanoparticles (quantum dots) to create microgel-nanoparticle hybrids [16–19]. By embedding nanoparticles within the matrices of responsive microgels, the long-term stability of nanoparticles is enhanced [16–22]. Furthermore, the optical and catalytic properties of nanoparticles can be modulated by stimuli-responsive parameters, opening up numerous applications [23–30]. The combination of stimuli-responsive behavior, easy synthesis, and the ability to incorporate nanoparticles makes PNIPAM microgels a highly attractive platform for studying fundamental phenomena and developing advanced materials for various applications in fields ranging from biomedicine to nanotechnology.

In context to our current studies on catalytic activities, PNIPAM microgel hybrids of Ag, Au nanoparticles have demonstrated excellent efficiency in the reduction of 4-nitro phenol to 4-aminophenol in the presence of excess sodium borohydride [16,22,31–38]. For example, Lu et al. [31] used core-shell microgel hybrids of Ag-nanoparticles in their work to show their catalytic activities, which they regulated through volume phase transition (VPT) of the thermosensitive shell and showed the variation of rate constant k from 0.05 to 0.24 min^{-1} for catalytic reduction reaction between temperatures range of 20–40 °C. Similarly Begum et al. [33] used Ag–P (NIPAM-co-AAm) hybrid microgels as catalyst for reduction of 4-nitro phenol, where they varied the concentration $NaBH_4$ and microgel Ag hybrid to achieve an optimum value of rate constant, i.e., 0.5 min^{-1}. Our group has also [16] used PNIPAM-AgNS hybrid as catalyst for nitrophenol reduction reaction and demonstrated a rate constant value of 0.159 min^{-1}.

It is to be noted that in most of the cases, catalytic studies have been carried out in the solution state where the efficiency of reusability of the materials decreases with increasing number of cycles due to possible aggregation in the solution and nanoparticles loose their surface properties. In the current studies we have implemented the concept of polymerized hydrogel materials (PGM), where the microgel@AgNP particles are confined within the polymer matrix [39]. By immobilizing the particles within the polymer matrix, the particles diffusion are ceased thus preventing the particle aggregation. This helps to thoroughly wash the PGM materials for its reuse in cyclic studies. Thus preventing the decrease in the catalytic efficiency in different cycles. The concept of polymerized hydrogels have been implemented only in very few catalytic studies. For example, Şahiner et al. demonstrated that metal nanoparticles could be formed in situ in chemical hydrogels and function as catalysis for hydrogel production by metal-catalyzed reduction of nitrophenols [34] or hydrolysis of sodium borohydride-based medium [35]. In some other reduction studies gold nanoparticles have been incorporated into the hydrogel matrix [36,37]. Chen et al. has demonstrated Ag composite responsive hydrogel for catalysis of 4-nitro phenol to amino phenol [38].

In this paper, we aim to inhibit the formation of particle aggregation during catalytic reactions, ultimately enhancing catalytic activity and efficiency. We plan to achieve this goal by encapsulating the catalysts within a polymerized gel material. This encapsulation strategy aims to prevent the undesired clustering of catalyst particles, ensuring their dispersion and active involvement in the reaction. By exploring the use of polymerized gel materials, we anticipate improved control over catalyst behavior, leading to enhanced overall performance in catalytic processes.This enhancement in catalytic efficiency can lead to improved reaction rates, increased product yields, and overall better performance of the catalytic system.

2. Experimental section

2.1. Materials and methods

Analytical reagent-grade chemicals including N-isopropylacrylamide (NIPAM), acrylic acid (AAC, 99%), N,N′-methylene-bis-

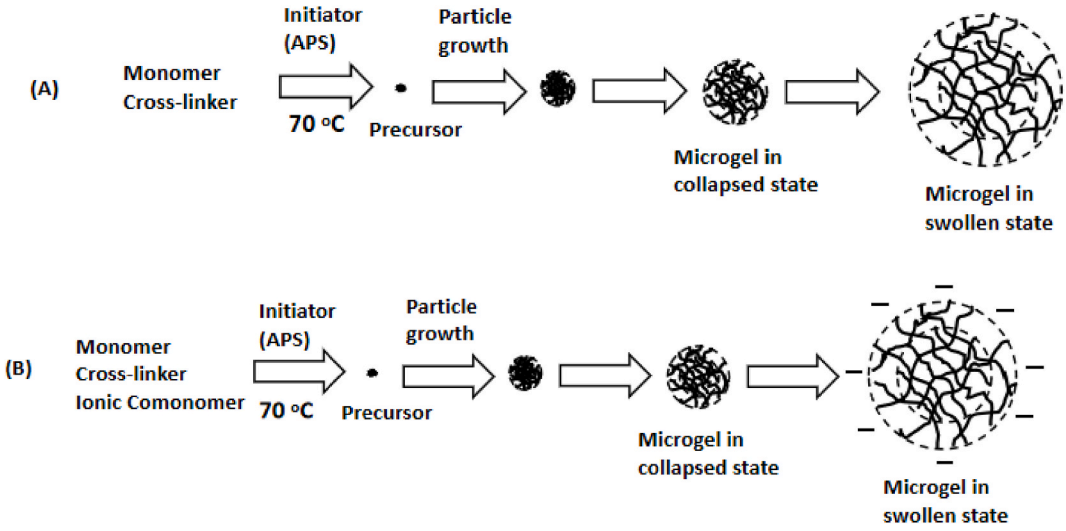

Fig. 1. Schematic representation of synthesis of **(A)** Thermo-responsive PNIPAM microgel and **(B)** pH & thermo-responsive Poly(N-isopropyl acrylamide-*co*-acrylic acid) microgel.

acrylamide (BIS, 97%), ammonium persulfate, 2,2′-Azobis (2-amidinopropane) dihydrochloride, sodium borohydride ($NaBH_4$), silver nitrate ($AgNO_3$), trisodium citrate, and 4-nitrophenol (4-NP) were obtained from Sigma, India. Mili-Q water was used exclusively throughout the experiment. UV-VIS absorption spectra were recorded using an in-house Cary 60 spectrometer from Agilent Technology. The wavelength scan interval was set at 1 nm with an accuracy of 0.015 nm.

All light scattering measurements were conducted using an in-house facility called the "Goniometer-based Multi-Angle Static and Dynamic Scattering Instrument" provided by Photocore Ltd in Russia. The scattering angle could be controlled using a stepper motor, ranging from 10° to 150° with an accuracy of 0.01°. The sample was immersed in a toluene bath, allowing for temperature variations between 10 °C and 90 °C with an accuracy of 0.1 °C.

Transmission electron microscope (TEM) images were obtained using a JEOL JEM-1400 instrument equipped with a tungsten filament. The microscope operated at an accelerated voltage of 80 kV and was located at CIPET, Bhubaneswar, India.

2.2. Synthesis of microgel

We followed the standard surfactant free precipitation polymerization process to synthesize thermoresponsive PNIPAM microgel, as described in our previous work [7,16,17]. As shown in Fig. 1 (A), N-isopropylacrylamide (NIPAM), N N, methylene-bis-acrylamide (BIS) and ammonium persulphate (APS) are used as monomer, cross linker and initiator respectively in the polymerization process. Once the synthesis process completed, purification of microgel suspension was done by multiple washing with MiliQ water by centrifugation followed by dialysis. In next step, we synthesized both pH and thermo-responsive microgel by using acrylic acid as ionic co-monomer as reported in our previous work [39] which is shown in Fig. 1 (B).

2.3. Synthesis of Ag NPs

In this step, Ag nanoparticles were synthesized by the conventional chemical reduction method, where silver nitrate ($AgNO_3$) as salt, sodium borohydride ($NaBH_4$) as the reducing agent and trisodium citrate (TSC) as stabilizing agent were used in the chemical reduction process. The reduction process was initiated by adding $NaBH_4$ drop-wise to mixture of $AgNO_3$ and TSC at room temperature under constant stirring condition. The addition of $NaBH_4$ has resulted rapid color change of the transparent solution to yellow that give the indication of the formation of AgNPs in the solution. The fig. 2 diagram represents the reduction process that results in the formation of Ag-atoms from Ag-ions and which leads to formation of Ag-nuclei and subsequent growth to form Ag-nanoparticles.

2.4. Synthesis of microgel@Ag hybrids

In this step, microgel@Ag hybrids were synthesized in in-situ method by the conventional reduction reaction process, where $NaBH_4$ was used as the reducing agent (see the fig. 3). The PNIPAM microgel beads were initially dispersed in distilled water. Then $AgNO_3$ solution was added to the PNIPAM microgel bead dispersion. Subsequently, $NaBH_4$ aqueous solution was added to the reaction mixture while maintaining constant stirring. The stirring process continued for an additional 15 min to ensure the completion of the reaction. A color change from colorless to pale yellow was observed immediately after the addition of $NaBH_4$. This color change indicated the formation of AgNS. The resulting microgel-Ag hybrids were purified by washing them twice with distilled water through centrifugation at 5000 rpm for 15 min.

2.5. Synthesis of polymerized gel materials (PGM)

We followed the standard protocol (see the fig. 4) for preparation of polymerized gel materials (PGM), as mentioned in our earlier work [39]. Firstly,we prepared the reaction mixture solution by taking required concentration of microgel Ag hybrid nanoparticles, monomer (acrylamide), cross-linker(BIS) and UV-initiator(2,2′-Azobis (2-amidinopropane) dihydrochloride). After mixing it well, the solution was kept undisturbed under UV light for polymerization with the help of a slide chamber. It took around 20–30 min for complete polymerization. After that the PGM was kept in Mili-Q water for overnight to attain the equilibrium swollen state to use in catalytic study. Through out the study, we maintained the PGM size as 1.2 cm × 1 cm x 0.3 cm. Fig. 5 represents the visual appearance of all the synthesized materials with their schematic representation.

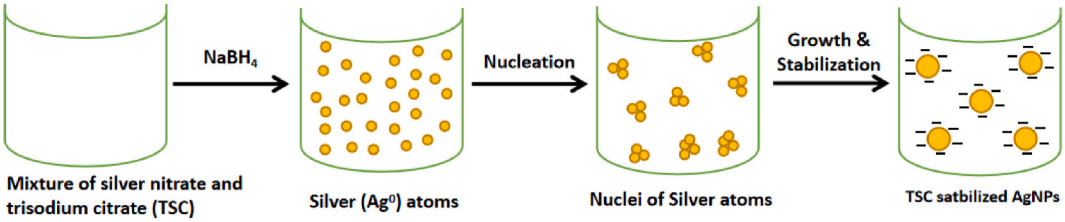

Fig. 2. Schematic representation of synthesis of AgNp using chemical reduction method with TSC as stabilizer and $NaBH_4$.

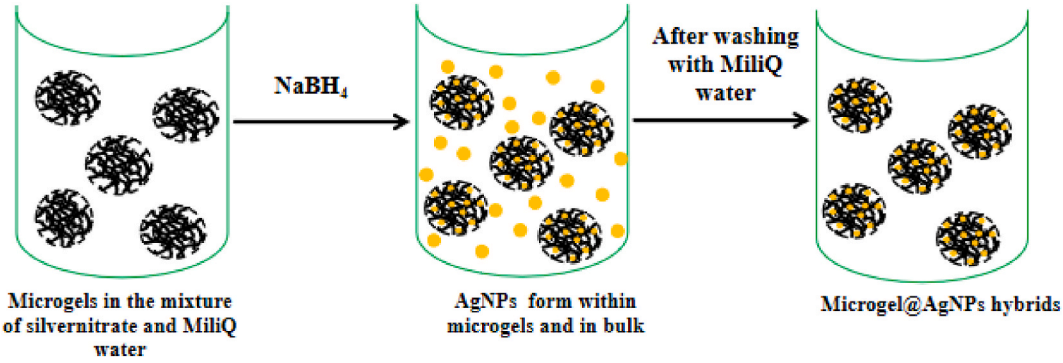

Fig. 3. Schematic representation of synthesis of microgel@AgNp in an in-situ treatment via chemical reduction method with $NaBH_4$ as reducing agent.

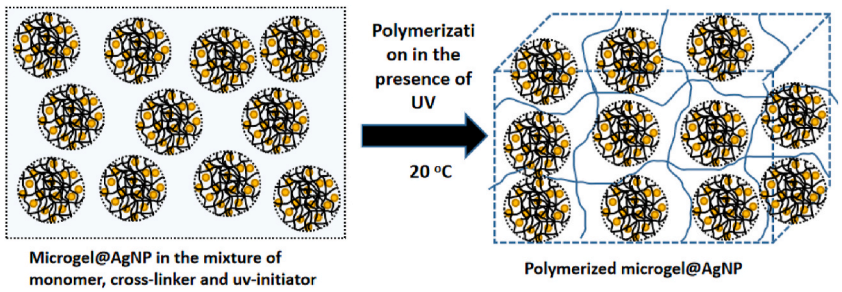

Fig. 4. Schematic representation of synthesis of polymerized microgel@AgNp (PGM@AgNP) via UV-polymerization method.

2.6. Catalytic reduction of 4-nitrophenol to 4-aminophenol

Reduction studies of 4-NP to 4-AP in presence of excess $NaBH_4$ were carried out using different materials mentioned in Fig. 5. UV–Vis spectroscopy was used to monitor the reduction process as a function of time. About 2.7 ml of distilled water was taken in a quartz cuvette having a path length of 1 cm, to which 20 μl of 0.01 M 4-nitrophenol solution was added. The reaction mixture was then

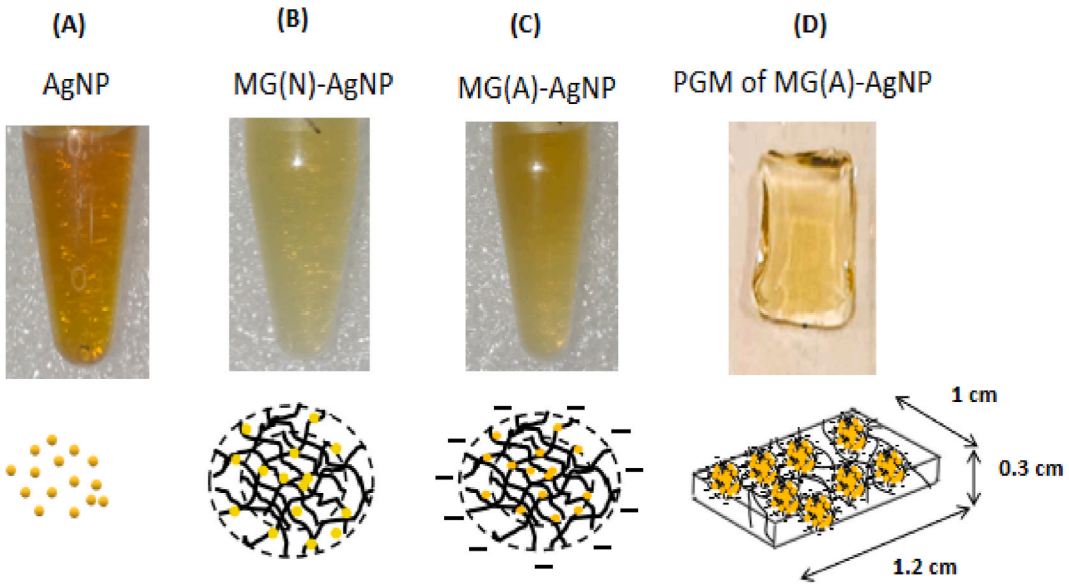

Fig. 5. Material prepared under different Figs. 2–4 of (A) pure AgNP, (B) MG (N)-@AgNP hybrid (Neutral), (C) MG(A)@AgNP hybrid (anionic), (D) PGM@MG(A)-AgNP.

allowed on gentle stirring followed by addition of the desired amount of catalyst. Finally, 250 μl of freshly prepared 0.15 M of $NaBH_4$ solution was added all at once and then the cuvette was left undisturbed till the end of the reaction for UV–Vis spectral measurement at different time intervals. The decrease in the peak intensity at 400 nm and increase in the peak intensity at 300 nm due to the catalytic conversion of 4-nitrophenolate ion to 4-aminophenol was observed for calculating reaction kinetics.

2.7. Dynamic light scattering

We utilized dynamic light scattering (DLS) studies to determine particle size distribution, where we measured the hydrodynamic radius according to the standard protocol [16,17]. For DLS studies, microgel suspensions are prepared at very dilute concentrations (~0.001 wt%), where particle interactions are minimized. Experiments are carried out using laser light of a specific wavelength (λ = 654 nm), and the fluctuations of scattered light are detected at a scattering angle of 90° using a photon detector. The time-dependent intensity-intensity correlation function is calculated from the fluctuations in scattering intensity at a given scattering vector at a given scattering angle [40]. The field correlation function, $g^1(\tau)$ is calculated from the intensity-intensity correlations and is then fitted to a distribution of decay rates, G(Γ), using equation,

$$g^1(\tau) = \int_0^\infty G(\Gamma) e^{-\Gamma\tau} d\Gamma \tag{1}$$

$$\Gamma = D_o q^2 \tag{2}$$

Here, Γ is the characteristic decay rate,τ is the delay time, q is scattering vector.
The translation free diffusion coefficient, D_o is given by using the Stokes-Einstein equation:

$$D_0 = \frac{k_B T}{6 \pi \eta R_h} \tag{3}$$

Where, k_B is Boltzmann constant, T is the absolute temperature, and η is the viscosity of the solvent. R_h is hydrodynamic radius of

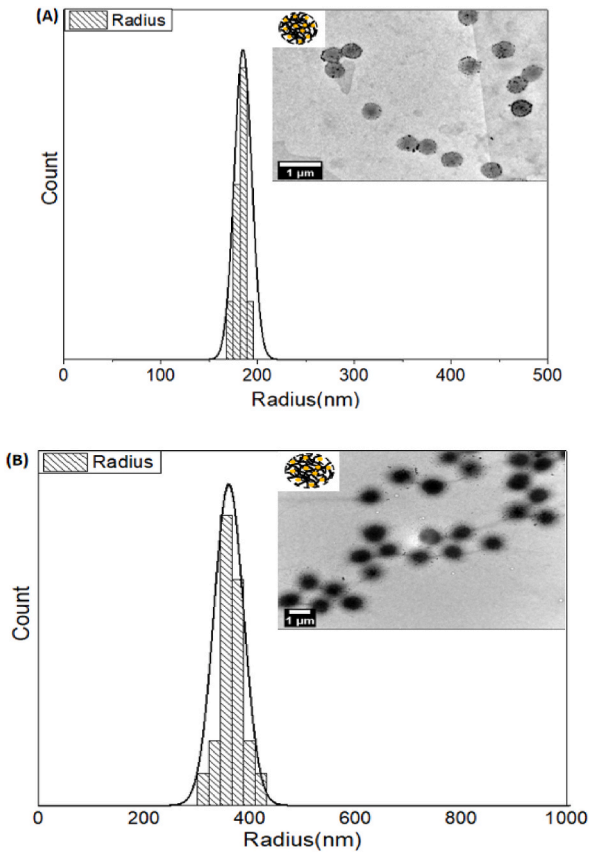

Fig. 6. Transmission electron microscope image in dried state with scale bar and the corresponding size distribution of **(A)** MG(N)–Ag hybrid particle with scale bar 1 μm and **(B)** MG(A)-Ag hybrids with 1 μm. The solid black line is the fitted Gaussian distribution.

particles.

3. Results and discussion

3.1. Characterizations of microgel@AgNP hybrids

PNIPAM-AgNP hybrid microgels were characterized with respect to the particle size distribution using transmission electron microscope (TEM) in the deswollen state, dynamic light scattering (DLS) in the swollen state and optical properties using UV–Vis spectroscopy.

Particle size distribution using TEM and DLS: TEM studies were carried out on both neutral microgel-silver hybrid particles [MG(N)–Ag] & anionic microgel-silver hybrid particles [MG(A)-Ag] in the dried state. TEM images clearly demonstrated the successful encapsulation of AgNPs within the microgel particles and the narrow size distribution of hybrid microgels.

It will be interesting to note that Fig. 6(A) shows a homogeneous distribution of Ag-nanoparticles within the neutral microgel particle, whereas in case of anionic microgel-Ag hybrid, the Ag-nanoparticles are distributed inhomogeneously within core and shell region of anionic microgel (Fig. 6(B)). Although in both cases, the Ag nanoparticles are grown within the network of microgel using in-situ synthesis method, anionic microgel produces core-shell structure of the hybrid particles. This variation in the distribution of Ag nanoparticles within the microgel is mostly due to inhomogeneous core-shell structure of the anionic microgel which has been observed in earlier work [41]. The particle size distribution for both hybrids were obtained from the image analysis using ImageJ software. The mean radius and standard deviation were obtained by fitting the distribution curves to a probability distribution of Gaussian type,

$$G = G_0 + Ae^{\frac{-(x-x_m)^2}{2w^2}} \tag{4}$$

Where G is the function,G_0 and A are standard constants, x_m is the mean value, w is the standard deviation.

From the fit the mean radius of MG(N)–Ag is found to be $x_m = 185 \pm 9$ nm as shown in Fig. 6(A) and that of MG (A)-Ag is found to be $x_m = 360 \pm 25$ nm as shown in Fig. 6(B). Due to lack of resolution of TEM, it is difficult to estimate the size distribution of Ag-nanoparticles within the microgel particles. The anionic microgel hybrid has a higher radius compared to the case of neutral microgel hybrid.

Although TEM studies demonstrated the narrow size distribution of hybrid particles, it didn't represent the true solution state structure that were used as catalysts. As the particles were soft and polymeric, the deswelling occur through drying and the TEM size did not represent the true solution state structure of the hybrid particles. The solution state structure of the hybrid particle were responsible for the catalytic activity.

In the next step, we implemented dynamic light scattering to study the swollen size of the hybrid of microgels in solution state at 20 °C. The distribution of hydrodynamic radius (R_h) of both hybrid microgels (MG(N)–Ag hybrid and MG(A)-Ag) along with the distribution of pure Ag-nanoparticles are plotted in Fig. 7. The mean radius of Ag NP, MG(N)–Ag hybrid and MG(A)-Ag hybrid obtained from DLS are 45 nm, 202 nm and 462 nm respectively. The sizes obtained from TEM are comparatively smaller than DLS, as microgel hybrid particles are in collapsed state in the TEM studies. The hydrodynamic radius characterizes the effective size of particles in a solution, accounting for their dynamic behavior and interaction with the solvent molecules. On the other hand, the TEM radius provides information about the physical size of the particles in their dried state, without considering the presence of dangling chains of microgels and the solvent or the solvation layer [41]. Therefore, the TEM radius is typically smaller than the hydrodynamic radius because it does not include the swelling effects induced by the solvent in the solution state. As shown in Fig. 7, it becomes evident that there is a notable emergence of aggregate structures in the case of silver nanoparticles (Ag NPs). Conversely, no such aggregation is observed in the instances of MG(N)–Ag and MG(A)-Ag hybrids. This observation strongly suggests an improved level of stability and

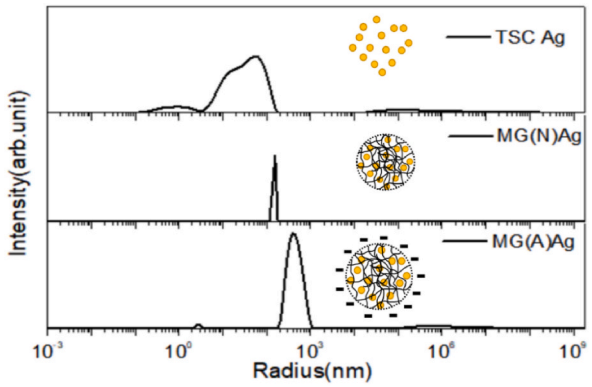

Fig. 7. Size distribution (Hydrodynamic radius) obtained from dynamic light scattering (DLS) of pure silver nanoparticles (AgNP), Neutral microgel-Ag hybrid [MG (N)–Ag] and Anionic microgel-Ag hybrid [MG (A)-Ag].

dispersion subsequent to the integration with microgel matrices. The occurrence of aggregation in the context of Ag NPs can be attributed to its heightened chemical reactivity. This elevated reactivity renders the nanoparticles susceptible to rapid oxidation, leading to rusting in the absence of any stabilizing agents. So we can say our microgel template provides better stability in formation of microgel Ag-hybrids, which is one of the main advantage of microgel hybrid particles.

In our previous work [42] molecular docking investigations were conducted to examine the interactions between various metal ions (Au^{3+}, Ag^{+}, Fe^{2+}) and their corresponding atomic states (Au^{0}, Ag^{0}, Fe^{0}), with the functional constituents of the polymer, specifically the NIPAM monomer and carboxylate ion (COO^{-}). The outcomes of these docking simulations revealed that electrostatic interactions play a predominant role, surpassing other types of interactions such as van der Waals forces, hydrophobic interactions, solvation effects, and electrostatic forces. The resulting net binding energies were determined to be −1.46 kcal/mol for Ag^{+} ions.

It is noteworthy that the cross-linked microgel particle matrices play a vital role in creating a confinement effect, effectively immobilizing the nanoparticles within the matrix. Additionally, the robust electrostatic interactions observed serve as an additional crucial mechanism contributing to the stability of the polymer-nanoparticle complexes. These interactions contribute significantly to the formation of stable complexes between the polymer and nanoparticles, thus fostering the creation of stable microgel-metal hybrid structures.

3.2. Optical properties

The formation of different nano-catalysts were confirmed by their colour changes during the synthesis. The absorption properties of all the catalysts were studied using UV–Vis spectroscopy as shown in Fig. 8. Ag Np showing a plasmonic peak at 400 nm confirmed the formation of Ag NP. Both PNIPAM and PNIPAM-co-AAc microgel stabilized hybrid Ag NPs shows peak around 420 nm, which confirms the formation of microgel-Ag hybrids, as the microgels do not have any absorption peak. Microgel-Ag experiences a significant 20 nm shift in its Plasmon band. This observable shift can be directly linked to the change of the PNIPAM microgel, an effect induced by the incorporation of silver particles within its structure [43]. In order to maintain same concentration of nano-catalysts for each during the catalytic reaction, we calibrate the concentration of each of catalysts and then used desired amount of catalyst from each one of them. Fig. 8 shows the absorbance of the exact amount of all the catalysts used in catalytic reaction. The peak observed in the case of Ag nanoparticles (Ag NPs) appears comparatively broader when compared to the narrower peak exhibited by MG Ag hybrids. This disparity signifies the presence of varying particle sizes, indicating a certain degree of polydispersity in case of Ag NPs. This phenomenon can be attributed to the occurrence of aggregation, resulting in the uneven distribution of particle sizes within the Ag NP sample.

3.3. Catalytic activity

In this study, 4-nitrophenol is used as model reactant for reduction in the presence of excess sodium borohydride ($NaBH_4$), which is a versatile system and has been used in many literatures due to its industrial importance in the study of waste water pollutant treatment [44]. In addition to that, since nitrophenol and aminophenol have absorption peak around 400 nm and 300 nm respectively, so UV–Vis spectrometer can be easily used to study the reduction of nitrophenol-to-aminophenol.With this motivation, we investigated the catalytic activities of our PGM containing MG(A)-Ag NP hybrids, using 4-NP in the presence of excess sodium borohydride. For comparison purpose, we also investigated the catalytic activity of Ag NP, MG(N)–AgNP and MG(A)-AgNP in bulk solution, by taking same concentration of nano-catalyst in each one of them as that of present in PGM as shown in Fig. 9.

In a typical reduction of 4-NP to 4-AP study, the UV–Vis spectra is measured as a function of time (Fig. 9). The absorption peak of 4-NP and 4-AP occurs at 400 nm and 300 nm respectively. At time t = 0, there is no formation of aminophenol and hence only one peak appears in the spectra at 400 nm for all the case due to the presence of nitrophenolate ion in alkaline medium. By the time, the peak at

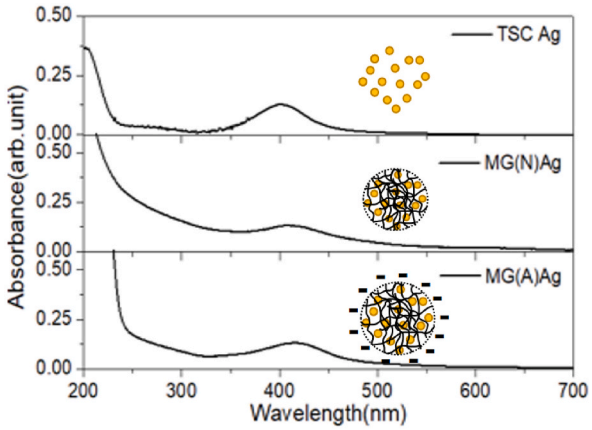

Fig. 8. UV–Vis absorption spectra of Ag NP in bulk, MG(N)–Ag and MG(A)-Ag (Respectively from top to bottom).

400 nm gradually decreases due to the reduction of nitrophenol and a new absorption peak appears at 300 nm due to the formation of aminophenol. As time proceeds, more amount of 4-NP reduce to 4-AP. Hence the height of absorption peak at 400 nm decreases and the peak at 300 nm increases as a function of time. After the complete reduction only the peak at 300 nm exists. With respect to the visual observation, the color of the sample changes from yellowish (at time = 0) to colourless after complete reduction indicating the formation of 4-AP. One can observe from Fig. 4, for the same concentration of nano-catalyst the complete reduction time of 4-NP to 4-AP varies for each one of them. For only AgNP, the complete reduction occurs in 30 min whereas it took 28 min for MG(N)–Ag NP, and 15 min for both MG(A)-Ag NP and PGM with MG(A)-Ag NP (Fig. 9).

Then to bring the practical applicability of the material, we investigated the re-useable properties of the PGM materials through cyclic catalytic activity for the same reduction reaction by using the same PGM of MG(A)-Ag NP. We observed that re-usability of the PGM material is very much possible. We did the re-usability check without any external triggering parameter and it took a little longer time as compared to the 1st cycle for complete reduction of 4-NP because of the slow diffusion of nitrophenol into the PGM matrix. Despite this prolonged duration, it is noteworthy that in each recycle test, the efficiency of the conversion of 4-NP to 4-Aminophenol (4-AP) remained consistently at 100%.

One way to quantify the conversion degree of nitrophenol to aminophenol is by comparing the concentration of nitrophenol C_t, at a specific time t, to its initial concentration C_0, at t = 0. This concentration ratio C_t/C_0, correlates with the ratio of the absorbance peak heights, A_t/A_0.

The apparent rate constant, k_{app}, associated with the reduction process, is directly proportional to the surface area S, of the nanoparticles per unit volume in the system [21].

$$-\frac{dC_t}{dt} = k_{app}\, C_t = k_1 S C_t \tag{5}$$

where C_t is the concentration of 4-NP at time t, k_{app} is apparent rate constant, k_1 is the rate constant normalized to surface area S. The above kinetic equation can be solved through integration as,

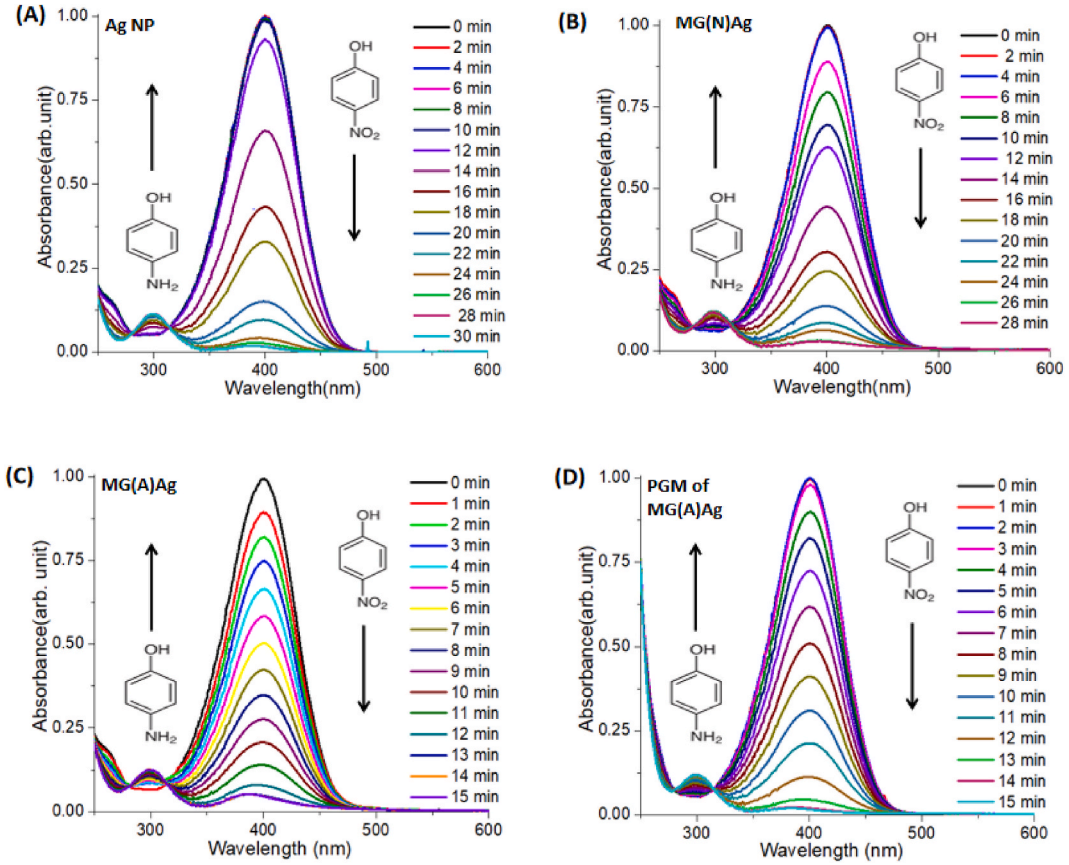

Fig. 9. Kinetics of UV–Vis spectra for reduction of 4-nitrophenol to 4-aminophenol by sodium bororhydride ($NaBH_4$) in presence of different catalyst **(A)** Ag NP **(B)** MG(N)–Ag NP, **(C)** MG(A)-Ag NP and **(D)** PGM with MG(A)-Ag NP. The interval in wavelength scan of UV–Vis spectra is 1 nm with accuracy of ±0.015 nm.

$$\int_{C_o}^{C_t} \frac{dC_t}{Ct} = -k_{app} \int_o^t dt \tag{6}$$

$$In\frac{C_t}{Co} = -k_{app}t \tag{7}$$

$$In\frac{A_t}{Ao} = -k_{app}t \tag{8}$$

Where A_0 and A_t represents the absorbance peak height at initial point and after t time respectively.

Hence the kinetics of the reduction process is analyzed by plotting $\ln(A_t/A_0)$ vs. reaction time (t) for different catalyst as shown in Fig. 10, where A_t and A_0 denote the absorbance at 400 nm at time t = t and at t = 0 respectively. When the concentration of sodium borohydride is higher than that of 4-nitrophenol, the reaction is expected to follow first-order kinetics [46]. However, in the case of certain catalysts, a pseudo-first-order reaction is also observed. Initially, the reaction exhibits an induction period denoted as t_0 (shown as a vertical dotted line in Fig. 10). This period can be referred to as the adsorption time or induction time [32,46]. After 4-nitrophenol is adsorbed onto the catalyst's surface, the reduction process begins slowly. It has been observed that the induction period varies across different catalysts, ranging from 0.5 min to several minutes shown in Fig. 11(A). Similar variations in induction time and their temperature dependence have also been noted for different Au-basd systems [45]. Higher value of induction time indicates slow reaction and vice versa. As here we investigate the catalytic reaction with different types of catalysts, we encountered different values of induction time for different catalysts as shown in Fig. 11(A). In case of pure Ag NP we found the reaction took almost 12 min to start. As we moved from PNIPAM-Ag hybrids to PNIPAM-co-AAc -Ag hybrids the induction time of the reaction drastically changes from 4 min to 0.5 min, indicating first reaction. But in case of PGM containing PNIPAM-co-AAc Ag hybrids the reaction took 3 min which is, slightly more than that for PNIPAM-co_AAc Ag hybrids this is because the slow diffusion of nitrophenols into PGM matrix.

Apparent rate constant, k_{app} is determined from the linear portion of $\ln(A_t/A_0)$ (the red line in Fig. 10) using equation (1). Interestingly, k_{app} is found to increase as we move from catalyst in bulk solution to the PGM form as shown in Fig. 11(B).

For experimental verification and wider applicability, we studied the re-usability of MG(A)-Ag in bulk and MG(A)-Ag within PGM. We repeated the catalytic reaction with same catalyst for different times. Fig. 12(A) shows the results of cyclic catalytic activity of bulk MG(A)-Ag and MG(A)-Ag within PGM under same condition. The percentage of conversion of bulk MG(A)-Ag found to be decreasing drastically with increase in number of cycle, whereas when the same MG(A)-Ag nanocatalysts were encapsulated within the matrix of PGM, the percentage of conversion remains close to 100% even after 3 cycle. The decrease in percentage of conversion of bulk MG(A)-Ag is due to the formation of aggregation after each reduction cycle. Fig. 12(B) shows the size distribution of MG(A)-Ag particles in bulk state, before and after 1st reduction cycle. From the distribution it is clear that a large amount of aggregate formed even after 1st cycle itself, which goes on increasing after each successive cycle which leads to decrease in percentage of conversion. After 3rd cycle the percentage of conversion of bulk MG(A)-Ag was found around 15% where in case of PGM with same catalyst, it was observed to be 100%. This interprets that, as compare to that of bulk solutions, the MG(A)-Ag nano particles were more stable inside the PGM matrix. They are less on the verge of loosing their surface properties, which leads to maximum conversion efficiency.

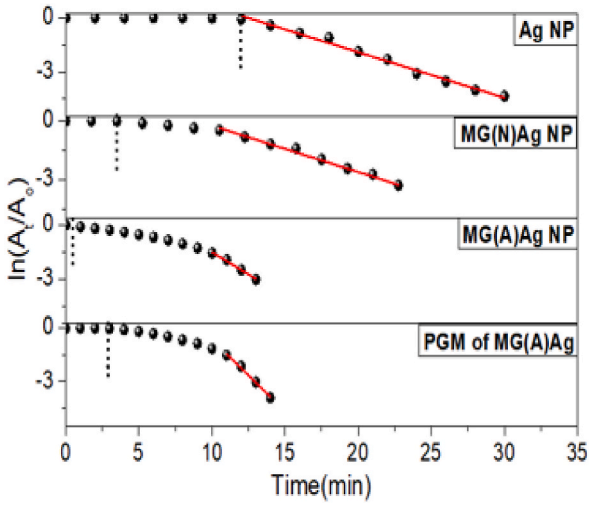

Fig. 10. Linear fitting of the data points obtained by plotting $\ln(A_t/A_0)$ vs time in the 4-nitrophenol reduction reaction in presence of sodium borohydride using different catalyst.

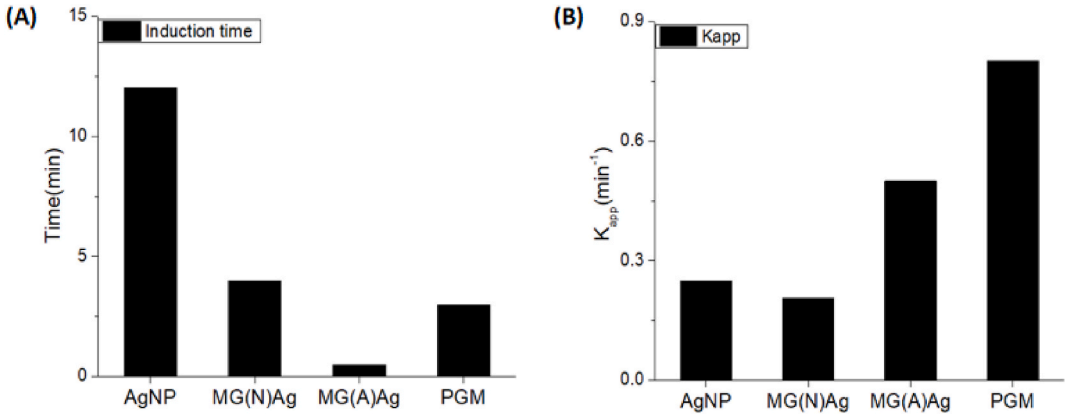

Fig. 11. Histogram showing **(A)** induction time and **(B)** apparent rate constant, K_{aap} as a function of different catalyst.

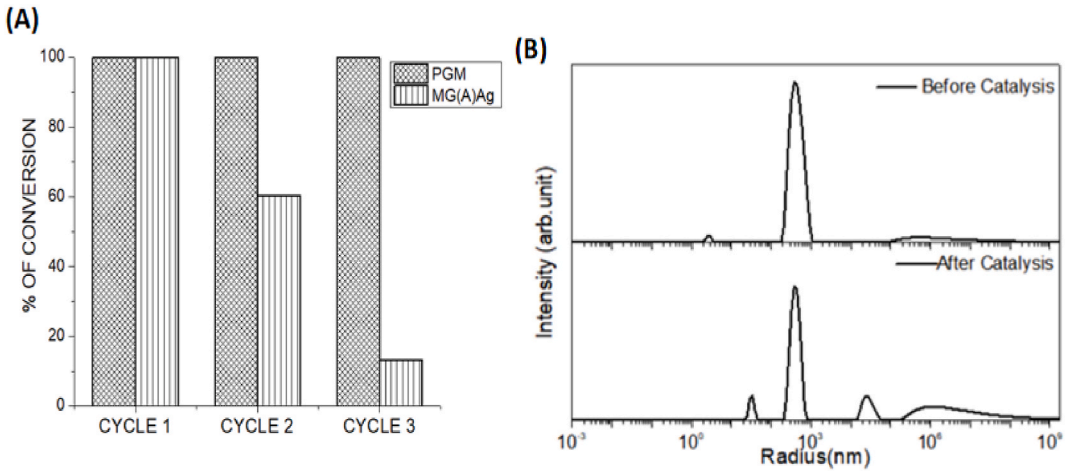

Fig. 12. **(A)** Percentage of conversion of catalytic reaction by PGM containing MG(A)-Ag and bulk MG(A)-Ag **(B)** Size distribution of MG(A)-Ag hybrid before catalysis (top) and after catalysis (bottom).

3.4. Discussion and comparison with other hybrids

Now, it will be interesting to discuss and compare our results with previously existing studies on catalytic activities of PNIPAM based microgel hybrids of Ag [16,31–38] and hydrogels containing metal nanoparticles [34–37]. Summary of comparison is given in Table 1. In our previous work [16] PNIPAM-Ag hybrid is used in suspension state for catalysis of 4-nitro phenol to amino phenol. The reaction took almost 30 min with an induction period of 7 min for complete reduction. The rate constant was found to be 0.159 min^{-1}. But under recyclability investigation we encountered a drastic drop in its efficiency. Lu et al. [31] in their study used a polystyrene core PNIPAM-Ag composite for catalysis. They varied the reaction temperature and found the highest rate constant as 0.21 min^{-1}. In

Table-1
Examining Related work for comparative Insights.

Hybrid Material	K_{app} (min^{-1})	Reusability efficiency	Reference
PNIPAM-Ag NS	0.159	poor	16
PS-NIPA-Ag composite	0.05 to 0.24	NA	31
poly(N-acryloylglycinamide)-AgNP	0.12	NA	32
PNIPAM-co-AAM-Ag	0.17–0.5	NA	33
p(AMPS)–Co hydrogel	0.075–0.2	good	34
p(AMPS)–Ni hydrogel	0.025–0.06	good	35
Au NP-PEGPU	0.084	Good with the help of regenerating agent	36
PNIPAM/Au nanocomposite hydrogels	0.017	NA	37
PNIPAM-GO-Ag hydrogel	0.1–0.26	NA	38
PGM of PNIPAM-co-AAc-Ag hybrid	0.8	Excellent	**This work**

another study Yang et al. [32] used poly(N-acryloylglycinamide)-Ag NP for catalysis purpose and observed a rate constant of 0.12 min^{-1}. Begum et al. [33] used PNIPAM-co-AAM -Ag hybrid in their study. They varied the sodium borohydride and hybrid catalyst concentration during catalytic reaction and reported a maximum rate constant of 0.5 min^{-1}. Shiner et al. [34,35] reported the preparation of soft hydrogels containing different metal nanoparticles such as cobalt, nickel etc. and their catalytic activity, where they have achieved very good efficiency over repeated recyclability test but these reactions took long time for complete conversion. Their reaction rate constant varies in the range of 0.075–0.2 min^{-1}. Similarly, Ramtenki et al. [36] reported the catalysis of 4-nitroaniline in presence of sodium borohydride by the help of gold nanoparticle embedded polyethylene glycolpolyoretane (PEGPU) hydrogel matrix. After 1st cycle they evaluated the rate constant to be 0.084 min^{-1}. They reported the aggregation of Au nanoparticles inside the hydrogel matrix after 3rd cycle. They used N-bromosuccinimide to regenerate the nanoparticles inside the matrix and used it for further catalytic activity. In another study Zhu et al. [37] reported the synthesis of PNIPAM-Au nano-composite hydrogel and checked its catalytic activity. The reaction took around 180 min for complete reduction of 4-nitro phenol with a rate constant of 0.017 min^{-1}. Chen et al. [38] synthesized PNIPAM@graphene oxide-Ag hydrogel [2 cm × 1 cm × 0.5 cm] for smart tunable smart catalytic activity. They used hydrogels of two different hybrid concentration and used at two different temperature. In their study they showed that for the higher concentration of hybrid hydrogel, with temperature the reaction rate constant increased up-to 0.26 min^{-1}. There is no report of recyclability of this material.

All of the above mentioned studies nicely demonstrated the excellent catalytic activity of PNIPAM-Ag or other PNIPAM metal hybrids. However most of the studies examined the catalytic activity in suspension state and reported about the decrease in efficiency over repeated cyclic activity. This decrease in efficiency is mainly due to the formation of aggregation after each step of catalytic reaction (see Fig. 13). Due to aggregation, nanoparticles loose their surface properties. This leads to decrease in efficiency, reusability and durability of the material. This is a main challenge in scaling up it into a material level for practical application.

By keeping all these points in view, our proposed polymerized hydrogel matrix containing PNIPAM microgel silver hybrids could provide additional novelty to the earlier work. In contrast to all the earlier reports, preparation method for our microgel hybrid and incorporating it into hydrogel matrix is quite easy and cost effective. Our proposed material exhibits excellent reusability and efficiency after several repeated cycle having a rate constant of 0.8 min^{-1} as compared to dispersion state as mentioned above. In addition to that our microgel hybrid exhibit both temperature and pH responsive properties. Here in this work we only focused on the efficient and successful reusability of the material for several repeated cycle. But it is possible to tune the catalytic activity with responsive parameters like pH and temperature with our microgel hybrids. Another advantage is that, the size of microgel hybrids and their responsiveness can also be tuned over a wide range by tuning the synthesis

approach. Thus, in case of our hybrid material, catalytic activity can also be further tuned based on various experimental parameters.

4. Conclusion & outlook

A simple and convenient method was employed for the preparation of Ag NP, PNIPAM-Ag hybrid and PNIPAM-co-AAc-Ag hybrid. The synthesized nanoparticles were characterized with UV–Vis absorption, TEM and dynamic light scattering studies. UV–Vis absorpion spectra shows the plasmon peak for all the nanoparticle hybrids. TEM image confirms the incorporation of nanoparticles into microgel and demonstrate its narrow size distribution. DLS gives the size of hybrid nanoparticles in swellen state at pH 7, 20 °C. Polymerization of hydrogel and incorporation of microgel-Ag hybrid within it is demonstrated. All the nanoparticles in suspension state and PGM containing MG(A)-Ag have been used as catalyst for the reduction of 4-nitrophenol to amino phenol. For bulk Ag NP, the first-order rate constant is found to be 0.25 min^{-1}, for PNIPAM-Ag NP hybrid (Neutral), it's 0.21 min^{-1} and for PNIPAM-co-AAc-Ag hybrid (Anionic), it's 0.5 min^{-1} where as for PGM containing anionic microgel hybrids it's found to be 0.8 min^{-1}. The induction period of Ag NP is 12 min, for MG(N)–Ag hybrid its 4 min, and for MG(A)g hybrid 30 s respectively. Similarly, for PGM containing MG(A)-Ag hybrid shows rate constant of 0.8 min^{-1} with 3 min induction period. So this study showed that the proposed material could be efficiently used as an efficient reusable catalytic material. Furthermore this reported procedure can be adapted to immobilize other nanoparticle hybrids into hydrogel matrix and use for different applications.

As our polymerized material demonstrates responsiveness to various stimulus parameters, such as temperature and pH, we aim to further explore its stimuli-responsive properties in subsequent stages. Specifically, we plan to investigate how changes in temperature and pH can be leveraged to achieve modulated catalytic activity.

CRediT authorship contribution statement

Biswajit Pany: Writing – original draft, Software, Methodology, Formal analysis, Data curation. **Amrito Ghosh Majumdar:** Writing – review & editing, Software, Methodology, Data curation. **Suresh Bhat:** Writing – review & editing. **Satybrata Si:** Writing – review & editing, Supervision. **Junpei Yamanaka:** Writing – review & editing, Supervision. **Priti S. Mohanty:** Writing – review & editing, Validation, Supervision, Project administration, Methodology, Data curation, Conceptualization.

Declaration of competing interest

The authors declare that they have no known competing financial interests or personal relationships that could have appeared to influence the work reported in this paper.

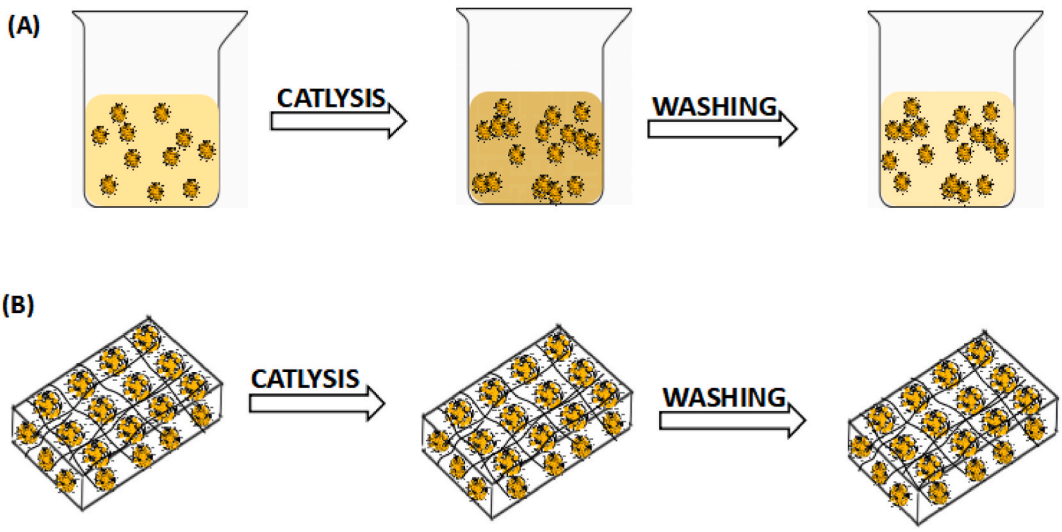

Fig. 13. Schematic representation of (A) Free microgel silver hybrids in suspension state (B) Encapsulated microgel silver hybrids inside the matrix of PGM.

Acknowledgements

P.S.M. acknowledges Core-Research Grant (CRG/2020/003086), SERB, Department of Science and Technology (India) for partial support.

References

[1] P. S. Mohanty and W. Richtering, J. Phys. Chem. B 2008, 112, 14692.
[2] P.S. Mohanty, S. Nojd, K. van Gruijthuijsen, J.J. Crassous, M. Obiols-Rabasa, R. Schweins, A. Stradner, P. Schurtenberger, Sci. Rep. 7 (2017) 1.
[3] P.S. Mohanty, P. Bagheri, S. Nojd, A. Yethiraj, P. Schurtenberger, Phys. Rev. 53 (2015) 011030.
[4] M. Murray, M. Snowden, Adv. Colloid Interface Sci. 54 (1995) 73.
[5] L.A. Lyon, A. Fernández-Nieves, Annu. Rev. Phys. Chem. 63 (2012) 25.
[6] H. Senff, W. Richtering, J. Chem. Phys. 111 (1999) 1705.
[7] P. S. Mohanty, D. Paloli, J. J. Crassous and P. Schurtenberger,Wiley, 2012, 369–395..
[8] T. Colla, P.S. Mohanty, S. Nojd, E. Bialik, A. Riede, P. Schurtenberger, C.N. Likos, ACS Nano 12 (2018) 4321.
[9] S. Xu, J. Zhang, C. Paquet, Y. Lin, E. Kumacheva, Adv. Funct. Mater. 13 (2003) 468.
[10] Y. Mei, Y. Lu, F. Polzer, M. Ballauff, M. Drechsler, Chem. Mater. 19 (2007) 1062.
[11] Y. Guan, Y. Zhang, Soft Matter 7 (2011) 6375.
[12] S. Petrusic, P. Jovancic, M. Lewandowski, S. Giraud, S. Grujic, S. Ostojic, J. Mater. Sci. 48 (2013) 7935.
[13] M. Yue, Y. Hoshino, Y. Ohshiro, K. Imamura, K, Y. Miura, Angew Chemie Int Ed 53 (2014) 2654.
[14] D. Sivakumaran, D. Maitland, T. Hoare, Biomacromolecules 12 (2011) 4112.
[15] T.R. Hoare, D.S. Kohane, Polymer (Guildf) 49 (2008) 1993.
[16] S.S. Satapathy, P. Bhol, A. Chakkarambath, J. Mohanta, K. Samantaray, S.K. Bhat, S.K. Panda, P.S. Mohanty, S. Si, Appl. Surf. Sci. 420 (2017) 75.
[17] R.K. Singh, P. Bhol, D. Mandal, P.S. Mohanty, J. Phys. Condens. Matter 32 (2019) 44001.
[18] J. Zhang, S. Xu, E. Kumacheva, J. Am. Chem. Soc. 126 (2004) 7908.
[19] Y. Lu, Y. Mei, M. Ballauff, M. Drechsler, J. Phys. Chem. B 110 (2006) 3930.
[20] R.W.J. Scott, O.M. Wilson, R.M. Crooks, J. Phys. Chem. B 109 (2) (2005) 692.
[21] M. Ballauff, Spherical polyelectrolyte brushes, Prog. Polym. Sci. 32 (2007) 1135.
[22] Timo Brandel, Viktor Sabadasch, Yvonne Hannappel, and Thomas Hellweg, ACS Omega**2019**, 4, 4636..
[23] C.D. Sorrell, M.C.D. Carter, M.J. Serpe, Adv. Funct. Mater. 21 (2011) 425.
[24] J. Zhang, S. Xu, E. Kumacheva, Adv Mater 17 (2005) 2336.
[25] Z.H. Farooqi, S.R. Khan, R. Begum, Mat. Sci. Technol. 33 (2017) 129.
[26] M. Ganguly, J. Jana, A. Pal, T. Pal, RSC advances 6 (2016) 17683.
[27] M. Fan, F. Lai, H.L. Chou, W.T. Lu, B.J. Hwang, A.G. Brolo, Chem. Sci. 4 (2013) 509.
[28] D. Suzuki, H. Kawaguchi, Langmuir 22 (2006) 3818.
[29] W. Wu, T. Zhou, A. Berliner, P. Banerjee, S. Zhou, Chem. Mater. 22 (2010) 1966.
[30] J. Zhang, N. Ma, F. Tang, Q. Cui, F. He, L. Li, ACS Appl. Mater. Interfaces 4 (2012) 1747.
[31] Y. Lu, Y. Mei, M. Drechsler, M. Ballauff, Angew Chemie Int Ed 45 (2006) 813.
[32] D. Yang, M. Viitasuo, F. Pooch, H. Tenhu, S. Hietala, Polym. Chem. 9 (2018) 517.
[33] R. Begum, et al., Appl. Organomet. Chem. 31 (2016) 2.
[34] N. Sahiner, et al., Appl. Catal. B Environ. 101 (1–2) (2010).
[35] N. Sahiner, et al., Appl. Catal. Gen. 385 (1–2) (2010).
[36] V. Ramtenki, et al., Colloids Surf. A Physicochem. Eng. Asp. (2012) 414.
[37] Zhu, C.-H. et al..Small, 2012,8(6)..
[38] J. Chen, Q. Luo, X.Z. Ma, J. Macromol. Sci., Part A 56 (10) (2019).
[39] B. Pany, et al., J. Mol. Liq. (2023) 375.
[40] B. J. Berne and R. Pecora, John Wiley and Sons, Inc., New York, 1976..

[41] P. Bhol, P.S. Mohanty, J. Phys. Condens. Matter 33 (8) (2020).
[42] P. Bhol, M. Mohanty, P.S. Mohanty, J. Mol. Liq. 325 (2021) 115135.
[43] Muhammad Siddiq, Khush Bakhat and Muhammad Ajmal Journal Pure and Applied Chemistry 92 (3) (2020) 445–459.
[44] T. Vincent, E. Guibal, Langmuir 19 (2003) 8475.
[45] J. Zeng, Q. Zhang, J. Chen and Y. Xia, Nano Letter**2010**, 10, 30-35..
[46] P. Hervé, M. Pérez-Lorenzo, L.M. Liz-Marzá, J. Dzubiella, Y. Lub, M. Ballauff, Chem. Soc. Rev. 41 (2012) 5577.